molecules

MDPI

Article

The Peroxymonocarbonate Anion HCO_4^- as an Effective Oxidant in the Gas Phase: A Mass Spectrometric and Theoretical Study on the Reaction with SO_2

Chiara Salvitti [1], Federico Pepi [1], Anna Troiani [1,*], Marzio Rosi [2] and Giulia de Petris [1,*]

[1] Dipartimento di Chimica e Tecnologie del Farmaco, "Sapienza" University of Rome, P.le Aldo Moro 5, 00185 Rome, Italy
[2] Dipartimento di Ingegneria Civile ed Ambientale, University of Perugia, Via Duranti 93, 06125 Perugia, Italy
* Correspondence: anna.troiani@uniroma1.it (A.T.); giulia.depetris@uniroma1.it (G.d.P.)

Abstract: The peroxymonocarbonate anion, HCO_4^-, the covalent adduct between the carbon dioxide and hydrogen peroxide anion, effectively reacts with SO_2 in the gas phase following three oxidative routes. Mass spectrometric and electronic structure calculations show that sulphur dioxide is oxidised through a common intermediate to the hydrogen sulphate anion, sulphur trioxide, and sulphur trioxide anion as primary products through formal HO_2^-, oxygen atom, and oxygen ion transfers. The hydrogen sulphite anion is also formed as a secondary product from the oxygen atom transfer path. The uncommon nucleophilic behaviour of HCO_4^- is disclosed by the Lewis acidic properties of SO_2, an amphiphilic molecule that forms intermediates with characteristic and diagnostic geometries with peroxymonocarbonate.

Keywords: peroxymonocarbonate anion; sulphur dioxide; oxidation reactions; electrospray ionisation mass spectrometry; ion–molecule reactions; theoretical calculations

check for updates

Citation: Salvitti, C.; Pepi, F.; Troiani, A.; Rosi, M.; de Petris, G. The Peroxymonocarbonate Anion HCO_4^- as an Effective Oxidant in the Gas Phase: A Mass Spectrometric and Theoretical Study on the Reaction with SO_2. *Molecules* **2023**, *28*, 132. https://doi.org/10.3390/molecules28010132

Academic Editor: Bryan M. Wong

Received: 24 November 2022
Revised: 16 December 2022
Accepted: 20 December 2022
Published: 23 December 2022

1. Introduction

The peroxymonocarbonate anion, HCO_4^-, was first isolated from alkali metal salts [1,2] and characterised by NMR, Raman spectroscopy [3], and X-ray crystallography [4] as the covalent adduct of the hydroperoxide anion HO_2^- and CO_2 ($HOOCO_2^-$). This anionic peracid, whose structure resembles that of analogous peroxo-species (e.g., peroxymonosulfate, peroxynitrate, and peroxyacetate) [5], is formed by the in situ reaction between hydrogen peroxide and bicarbonate at a near-neutral pH and in the absence of strong and corrosive acids [6]. Accordingly, bicarbonate-activated hydrogen peroxide (BAP) systems provide a source of HCO_4^- ions, which are employed as a selective electrophilic oxidant for electron-rich compounds including alkenes [7], amines [8], organic sulphides [9–11], and thiols [12]. HCO_4^- is also widely exploited in field-scale applications in environmental remediation processes [13,14] and water treatment [15]. No less important is its role in biological systems, where both hydrogen peroxide and bicarbonate are ubiquitous species in extracellular fluids [16,17]. Indeed, HCO_4^- has been indicated as a reactive oxygen species (ROS) in the two-electron oxidation of sulphur-containing aminoacidic residues [11,12], with important implications in neurodegenerative diseases [18] and in the peroxidase activity of copper and zinc superoxide dismutase enzymes (Cu, Zn-SOD) [19]. In most of the above cases, the peroxymonocarbonate ion acts as an electrophilic oxidant [7–13], while only a few studies report its behaviour as a nucleophile [20–23], although it is believed that the strong oxidant HOO^-, present in BAP systems, is the actual nucleophilic oxidant [14].

In contrast to the wealth of studies performed in solution, in the gas phase, to the best of our knowledge, only one study has reported the reactivity of an isobaric electrostatic ionic complex $[HO_2 \cdots CO_2]^-$ towards atmospheric constituents [24], suggesting the possible occurrence of a bound species, the peroxymonocarbonate ion.

In the gas phase, the peroxymonocarbonate anion has been known since 1977, when it was observed in a flame ionisation detector [25,26] upon clustering reactions involving free oxygen radicals with CO_2 or carbonate derivatives, and more recently in air plasma [27,28], either as a free species or as a negative core ion of large water clusters [29]. The lack of gas-phase reactivity studies concerning HCO_4^- ions prompted us to investigate the reactions of this anionic peracid in a joint mass spectrometric and theoretical approach. Over the years, this approach has provided a wealth of knowledge on the intrinsic reactivity of isolated ions towards neutral species in a pristine environment, i.e., in the absence of the masking effects of solvents or counter-ions typically operating in bulk environments [30–32]. We therefore undertook an investigation of the oxidative behaviour of HCO_4^- towards sulphur dioxide by ion trap mass spectrometry, exploiting an in-house-modified experimental set-up to perform ion–molecule reactions [33]. This experimental approach allows one to precisely ascertain the identity of the reactive (oxidant) species, as well as the relationship between the reagent (oxidant), intermediates and the products involved [30,31]. In the last few years, we have thoroughly investigated the reactivity of sulphur dioxide, one of the most produced commodity chemicals worldwide [34] and, at the same time, a harmful pollutant [35], with singly [36,37] and doubly charged [38–40] metal oxide anions and non-metal anionic oxides [41–44]. The very rich chemistry observed is the result of the amphoteric nature of SO_2, whose sulphur atom can either behave as an electron acceptor or as an electron donor. The nucleophilic ability is due to the lone pair on sulphur in a high-lying σ-based HOMO, whereas the electrophilic properties are due to the low-lying π-symmetry LUMO of sulphur dioxide [45]. Interestingly, the donor–acceptor behaviour of SO_2 is reflected in the diagnostic geometrical features of non-metal [46] and metal–SO_2 complexes [45,47].

We found that SO_2 was effectively oxidised by HCO_4^- to hydrogen sulphate, sulphur trioxide, and SO_3^-, together with carbon dioxide, hydrogen carbonate, and the hydrogen carbonate radical. Hydrogen sulphite was also observed as a result of a secondary reaction promoted by HCO_3^- [48]. Our study adds a new contribution to the gas-phase chemistry of both HCO_4^- and sulphur dioxide, highlighting the nucleophilic oxidative properties of peroxymonocarbonate, which are disclosed thanks to the electrophilic character of sulphur dioxide. A brief description of the generation of the anionic peroxide HCO_4^- by electrospray ionisation (ESI) in our experimental set-up is also given, whereas experiments on sulphur-containing molecules of atmospheric, environmental, and biological interest are ongoing in our laboratory.

2. Results

2.1. Formation and Characterisation of Peroxymonocarbonate Ion (HCO_4^-)

The peroxymonocarbonate ion (HCO_4^-) is typically obtained in solution through a substitution reaction between bicarbonate (HCO_3^-) and hydrogen peroxide (H_2O_2) [6,7,9], whereas, in the gas phase, different formation pathways that consist of the oxidation of the CO_2 or CO_3^- species have been proposed [25–28]. Accordingly, we generated the HCO_4^- ion by two alternative methods and precisely through the electrospray ionisation (ESI) of (1) a solution of sodium percarbonate ($Na_2CO_3 \cdot 1.5\ H_2O_2$; avail. H_2O_2 20–30%) or (2) pure water.

The first approach is advantageous as sodium percarbonate is known to be a stable and easy-to-handle, commercially available compound, providing at once proper amounts of HCO_3^- and H_2O_2 in water. The peroxymonocarbonate ion was indeed formed in $Na_2CO_3 \cdot 1.5\ H_2O_2$ solution and gently transferred to the gas-phase environment for structural and reactivity investigations.

The second option is also convenient since, by injecting pure water into the ESI source, line saturation effects and the need for frequent cleaning operations are avoided. Furthermore, the application of in-source electric fields to assess the ionisation process lead to the formation of different oxidising agents [49] that react with O_2 or CO_2 typically found in the ambient air or dissolved in water in different forms ($CO_{2(aq)}$, HCO_3^-). The

ESI approach is also a gentler ionisation method than atmospheric pressure chemical ionisation (APCI), which permits the application of a negative corona discharge in room air to obtain the HCO_4^- ion [27–29,50]. According to these studies, we also succeeded in generating the peroxymonocarbonate ion through the APCI of ambient air, but the electrospray ionisation of water proved to be the best approach to assess the stable ionic signal of the HCO_4^- species, which is a prerequisite for kinetic measurements. Interestingly, to the best of our knowledge, the formation of the HCO_4^- ion under these conditions has never been emphasised by other authors, since the studies analysing the ESI speciation of pure water mainly investigate the aggregation phenomena of $H^+(H_2O)_n$ and $OH^-(H_2O)_n$ cluster ions [51].

Focusing on the gas-phase formation pathways of the HCO_4^- ion, two different reactions were proposed, namely the three-body association reactions of (1) $CO_3^- + OH^\bullet + M$ and (2) $HO_2^- + CO_2 + M$ [25–29]. In our experimental conditions, the ESI-(–) mass spectrum of pure water acquired in the low 20–150 mass range shows (Figure 1), among others, intense ionic signals at *m/z* 32 ($O_2^{\bullet-}$), at *m/z* 50 (the hydrated cluster ion $[O_2 \cdot H_2O]^{\bullet-}$), and at *m/z* 60 corresponding to the CO_3^- ion. The HO_2^- species at *m/z* 33, commonly obtained through the discharge ionisation of H_2O/O_2 mixtures [52], is present only in a very low amount, as also already reported in the corona discharge ionisation systems by Ninomiya et al. [28], together with other ionic species also present in the ESI-(-) mass spectrum, but not involved in the formation of the HCO_4^- ion.

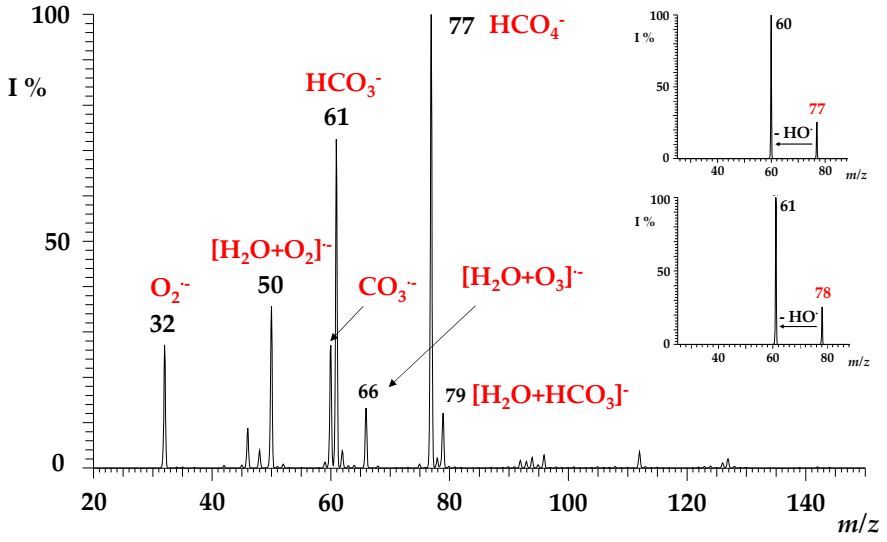

Figure 1. Mass spectrum for the electrospray of water acquired in the negative ion mode in the *m/z* range of 20–150. Inset: MS/MS of HCO_4^- ions at *m/z* = 77 (upper) and $H^{13}CO_4^-$ ions at *m/z* = 78 (lower). See text for details.

To evaluate the possible formation pathway occurring under ESI conditions, we carried out two different experiments. In the first, we infused aliquots of water (previously decarbonated) enriched with $Na_2{}^{13}CO_3$ or with $NaH^{13}CO_3$ as a source of $^{13}CO_3^-$ ion. As a result, the HCO_4^- ion at *m/z* 77 always largely predominates over the labelled $H^{13}CO_4^-$ species at *m/z* 78, even if the $H^{13}CO_3^-$ ion represents the base peak, thus excluding the $CO_3^- + OH^\cdot + M$ reaction as a possible HCO_4^- formation pathway.

In the second experiment, we analysed an aliquot of water previously degassed to eliminate the dissolved CO_2 and subsequently placed in a closed vessel saturated with $^{13}CO_2$ (P $^{13}CO_2$ = 700 torr). Although the occurrence of the $^{13}CO_{2(g)} \rightleftharpoons {}^{13}CO_{2(aq)} \rightleftharpoons H^{13}CO_3^-{}_{(aq)}$ equilibrium in water is unavoidable [53], a strong increase in the $H^{13}CO_4^-$ ion compared to its ^{12}C isotopologue was observed, highlighting the occurrence of the $HO_2^- + CO_2 + M$ reaction in the ESI generation of the peroxymonocarbonate ion. According to this hypothesis, the neutral CO_2, rather than CO_3^- or HCO_3^- ions, is supposed to be the oxidation target, as

demonstrated by the absence of an increase in the HCO_4^- ionic signal when water is enriched with bicarbonate or carbonate species, as previously described.

Interestingly, our results parallel the evidence of the intermediacy of CO_2 in bicarbonate/hydrogen peroxide solutions, where HCO_4^- is formed through CO_2 perhydration or base-catalysed perhydration [6,8,11].

Prior to investigating its gas-phase reactivity (see next paragraph), the HCO_4^- species was mass-selected and characterised by collision-induced dissociation (CID) experiments. The HCO_4^- ion at *m/z* 77 fragments by releasing a hydroxyl radical counterpart ($OH^\bullet$; 17 Da) [28], leading to the formation of a carbonate radical anion ($CO_3^{\bullet -}$) at *m/z* 60 (Figure 1, upper inset), which accounts for the higher EA of $CO_3^\bullet$ with respect to $HO^\bullet$ [54]. Likewise, the fragmentation of the ^{13}C-isotopologue $H^{13}CO_4^-$ at *m/z* 78 gives rise to the corresponding $^{13}CO_3^{\bullet -}$ species at *m/z* 61 (Figure 1, lower inset).

2.2. Reactivity of Peroxymonocarbonate Ion (HCO_4^-) towards Sulphur Dioxide (SO_2)

2.2.1. Mass Spectrometric Results

Regardless of the preparation method (if formed by electrospray ionisation of a percarbonate solution, of water, or of a saturated solution of $^{13}CO_2$), the peroxymonocarbonate HCO_4^- and its heavy ^{13}C-form predictably show superimposable reactivity towards sulphur dioxide. They were mass-selected and exposed to SO_2 in the ion trap cell to monitor the formation of ionic products as a function of the activation time. A typical product ion spectrum is reported in Figure 2, showing the formation of ionic signals at *m/z* 97, 81, 80, and 61, respectively, attributed to HSO_4^-, HSO_3^-, SO_3^-, and HCO_3^-. Ions at *m/z* 97 and 81 clearly contain one sulphur atom, as witnessed by the characteristic signature of the ^{34}S peak at [M + 2] ($H^{34}SO_4^-$ *m/z* = 99; $H^{34}SO_3^-$ *m/z* = 83), though not easily distinguishable for the low-intensity SO_3^- peak at *m/z* = 80.

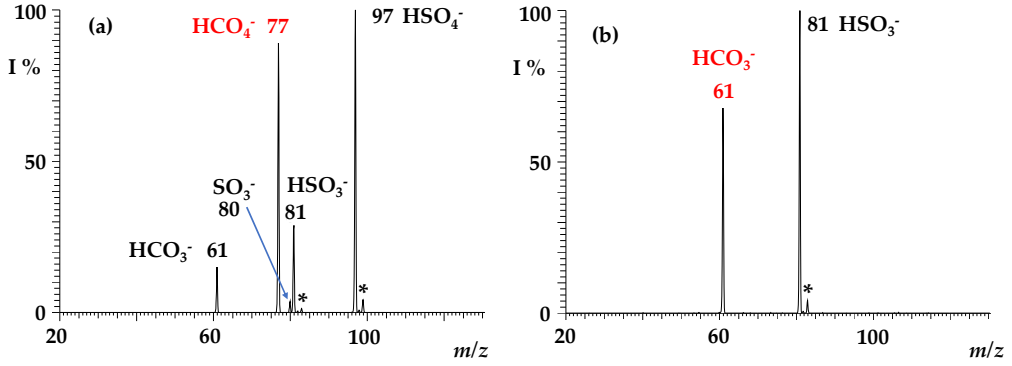

Figure 2. ITMS spectrum showing (**a**) the ion–molecule reaction of isolated HCO_4^- ions (*m/z* 77) with SO_2, reaction time = 200 ms, P SO_2 = 1.3 × 10^{-7} Torr. Observed products: HSO_4^- at *m/z* 97, HSO_3^- at *m/z* 81, HCO_3^- at *m/z* 61; the signals denoted with * correspond to $H^{34}SO_3^-$ (*m/z* = 83) and to $H^{34}SO_4^-$ (*m/z* = 99); (**b**) the ion–molecule reaction of HCO_3^- ions (*m/z* 61) isolated from the sequence 77 → 61 with SO_2 (reaction time = 200 ms, P SO_2 = 1.3 × 10^{-7} Torr), showing that HSO_3^- at *m/z* 81 is formed from a consecutive reaction. The signal denoted with * at *m/z* 83 corresponds to $H^{34}SO_3^-$.

The kinetic profile of the reaction (Figure 3) shows that products are formed through parallel and consecutive reactions, and that the precursor ion conversion is fast and efficient, with a decay constant k_{dec} at 298 K of 7.2 × 10^{-10} cm^3 $molecule^{-1}$ s^{-1} and efficiency (k/k_{coll}) of 54.8% (Table 1). Three parallel reaction pathways can be identified in the following:

$$HCO_4^- + SO_2 \rightarrow HSO_4^- + CO_2 \quad (1)$$

$$HCO_4^- + SO_2 \rightarrow HCO_3^- + SO_3 \quad (2)$$

$$HCO_4^- + SO_2 \rightarrow HCO_3 + SO_3^- \quad (3)$$

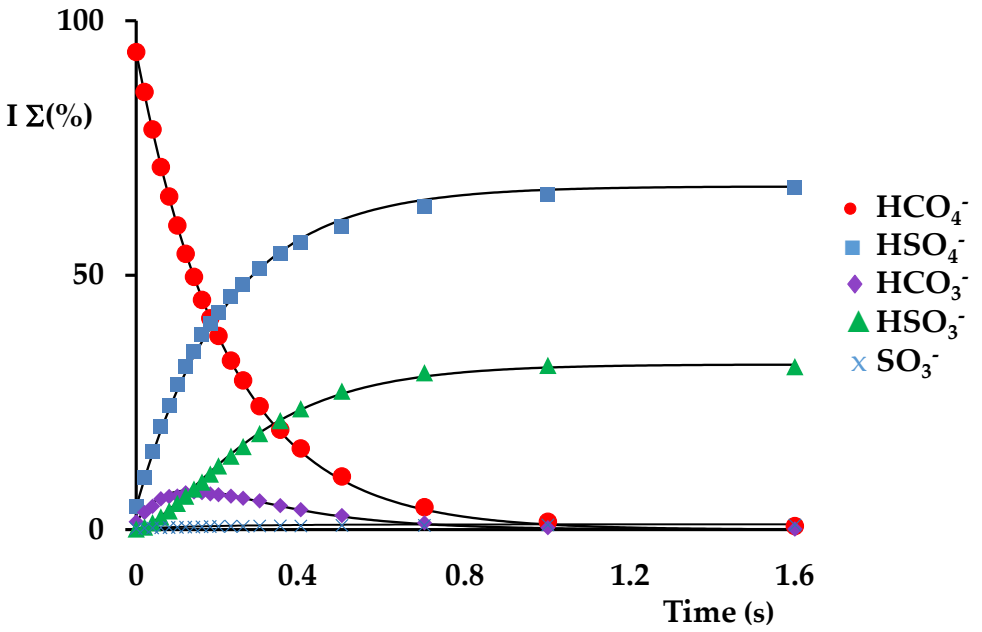

Figure 3. Kinetic plots and best fit lines of the reaction of isolated HCO_4^- ions (*m/z* 77) (P SO_2 = 1.97 × 10^{-7} Torr): ● HCO_4^- (R^2 = 0.9997), ■ HSO_4^- (R^2 = 0.9989); ▲ HSO_3^- (R^2 = 0.9946); ♦ HCO_3^- (R^2 = 0.9941); x SO_3^- (R^2 = 0.9764).

Table 1. Rate constants (cm^3 s^{-1} $molecule^{-1}$), efficiencies (%), and branching ratios (% Σ) relative to the reaction of HCO_4^- + SO_2. See text for rate constant numbering, k_n.

	Rate Const. (×10^{-10}) [a]	Eff.% [b]	Branching Ratio%
k_{dec}	7.2	54.8	
k_1	4.6	35.1	64.5
k_2	2.5	19.1	34.8
k_3	0.050	0.4	0.70
k_4	14.0 [c]	>100	

[a] ±30%; [b] k/k_{coll}; [c] see ref. [48].

The main reaction channel 1 consists of a formal SO_2/CO_2 switching, leading to the formation of the bisulphate HSO_4^- product ion at *m/z* 97, accounting for a branching ratio of 64.5% (k_1 = 4.6 × 10^{-10} cm^3 $molecule^{-1}$ s^{-1}) and efficiency of 35.1% (Table 1). From another point of view, this reaction can also be considered as a formal hydroperoxide anion HOO^- transfer. Pathway 2 gives rise to the HCO_3^- ion at *m/z* 61 with the release of SO_3 as the neutral counterpart through an oxygen atom transfer (OAT) reaction to SO_2 occurring with a rate constant of k_2 = 2.5 × 10^{-10} cm^3 $molecule^{-1}$ s^{-1} (eff. = 19.1%) and a branching ratio of 34.8%. Finally, the very minor path 3, accounting for less than 1% of the products, leads to SO_3^- at *m/z* 80, with a k_3 = 5.0 × 10^{-12} cm^3 $molecule^{-1}$ s^{-1} (reaction 3, eff. = 0.4%) through oxygen ion transfer (OIT). The preferential formation of products from reaction 2 with respect to those of reaction 3 accounts for the considerably higher electron affinity of the bicarbonate radical (EA HCO_3 = 3.68 eV) [55] with respect to SO_3 (EA SO_3 = 1.90 eV) [54].

The HCO_3^- ion formed by reaction 2 is known to be reactive towards SO_2 to form HSO_3^- [48], and indeed it is rapidly depleted in a consecutive reaction forming the bisulphite anion at *m/z* 81 and carbon dioxide (Equation (4)), as illustrated in Figure 2b.

$$HCO_3^- + SO_2 \rightarrow HSO_3^- + CO_2 \quad (4)$$

This process occurs at a collision rate, with a measured rate constant k_4 of 1.40 × 10^{-9} cm^3 $molecule^{-1}$ s^{-1} (Table 1), in good agreement with previous data [48]. Spectra relative to the reaction of the $H^{13}CO_4^-$ ion are reported in Figure S1 (Supplementary Materials).

The reaction of HCO_4^- + SO_2 → HSO_4^- + CO_2 described in Equation (1) is an irreversible process, since no displacement of SO_2 by CO_2 occurred when the HSO_4^- ion was reacted with CO_2, not even with the high pressure of carbon dioxide or extension of the activation time up to the maximum value of 10 s. Similar irreversible switching reactions were also observed in the gas phase by reacting carbonate cluster ions with SO_2 and resulting in the complete conversion of carbonate into sulphite ions [43].

2.2.2. Theoretical Calculations

The oxidation routes of SO_2 promoted by HCO_4^- were investigated using density functional calculations. Optimised geometries of relevant stationary points and transition states on the B3LYP/aug-cc-pV(T+d)Z potential energy surface for the processes are reported in Figure 4, while charge density distributions of relevant minima are shown in Figure 5. Complete geometrical parameters of minima and saddle points are shown in Figure S2 (Supplementary Materials). Enthalpy changes (kcal mol^{-1}) at 298.15 K computed at the B3LYP/aug-cc-pV(T+d)Z and CCSD(T)/aug-cc-pV(T+d)Z levels of theory are detailed in Table 2. In the following, only the CCSD(T) values will be considered.

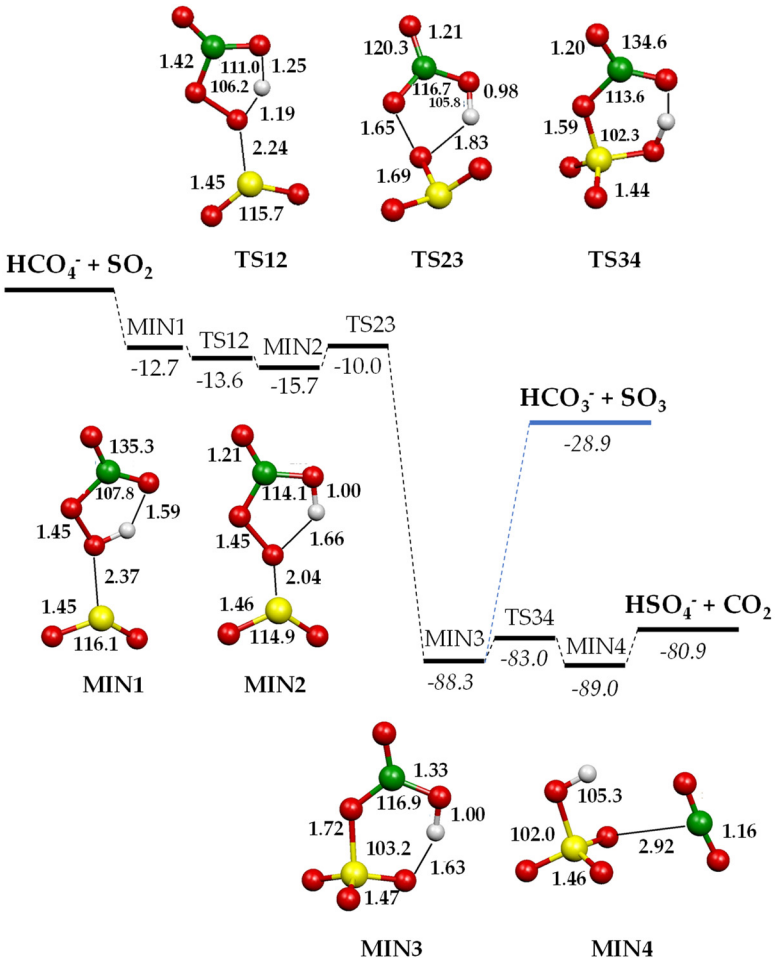

Figure 4. Schematic energy diagram of the reaction of HCO_4^- ions with SO_2. Geometries of the minima localised on the $[HCO_4 \cdots SO_2]^-$ potential energy surface optimised at the B3LYP/aug-cc-pV(T+d)Z level of theory. Bond lengths in Å, angles in degrees, ΔH° values in kcal mol^{-1} computed at the CCSD(T)/aug-cc-pV(T+d)Z level of theory.

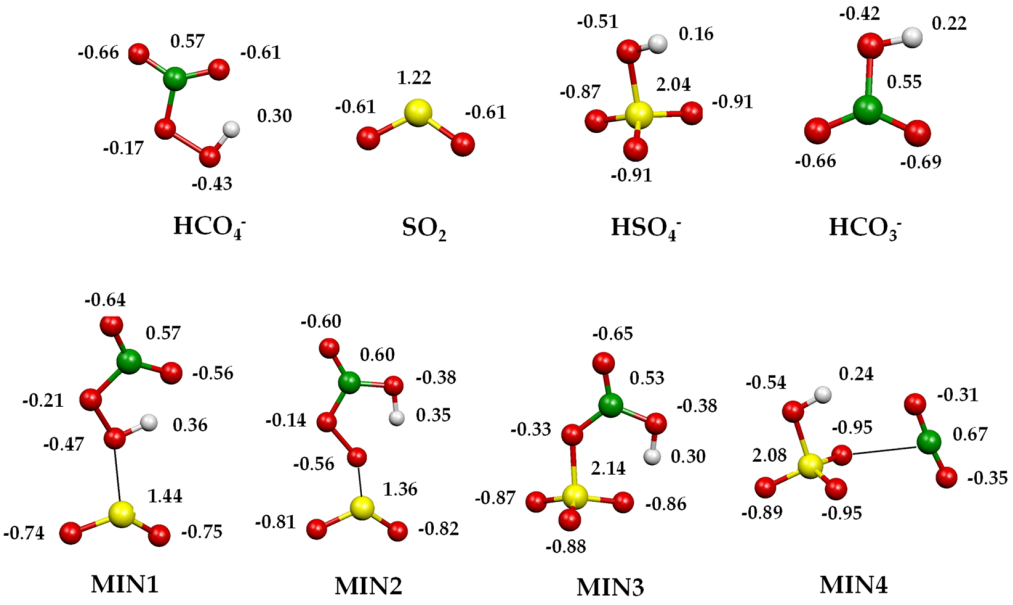

Figure 5. Charge density distributions of the minima and transition states localised on $[HCO_4 \cdots SO_2]^-$ potential energy surfaces computed at the CCSD(T)/aug-cc-pV(T+d)Z level of theory.

Table 2. Enthalpy changes (kcal mol^{-1}, 298.15 K) computed at the B3LYP/aug-cc-pV(T+d)Z and CCSD(T)/aug-cc-pV(T+d)Z levels of theory for selected reaction of HCO_4^- + SO_2.

	$\Delta H^\circ_{298.15}$		Barrier Height	
	B3LYP	**CCSD (T)**	**B3LYP**	**CCSD (T)**
$HCO_4^- + SO_2 \rightarrow HCO_3^- + SO_3$	−28.2	−28.9		
$HCO_4^- + SO_2 \rightarrow HCO_3 + SO_3^-$	−1.7	5.9		
$HCO_4^- + SO_2 \rightarrow HSO_4^- + CO_2$	−77.5	−81.0		
$HCO_4^- + SO_2 \rightarrow$ MIN1	−12.9	−12.7		
MIN1 → MIN2	−2.2	−3.0	−0.7	−0.9
MIN2 → MIN3	−65.8	−72.6	5.0	5.7
MIN3 → MIN4	−1.2	−0.7	4.8	5.3
MIN4 → $HSO_4^- + CO_2$	4.7	8.1		
MIN3 → $HCO_3^- + SO_3$	52.8	59.4		

HCO_4^- features a five-membered-ring intramolecular hydrogen bond between the carbonyl oxygen and the hydrogen atom bound to the peroxidic oxygen [28]. The initial attack of the peroxymonocarbonate anion involves this oxygen atom interacting with the incoming SO_2 and leads to an encounter complex (MIN1) stabilised by a binding energy of 12.7 kcal mol^{-1}. The two moieties, at a distance of 2.37 Å, almost conserve their original geometric features, with SO_2 binding to the peroxyl oxygen in a bent coordination mode: the angle between the peroxyl O–S bond vector and the SO_2 plane is around 100°, with the dihedral OSOO angle equal to 102.1°. With a negative small activation barrier, MIN1 converts to a slightly more stable MIN2, in which the proton is now bound to the carbonyl oxygen. The saddle point TS12 is highly stabilised by the sharing of the proton between the two oxygen atoms. In MIN2, the peroxidic O–S bond shortens to 2.04 Å, developing a small negative charge on SO_2 (−0.27 e^-) and still binding with a bent geometry (angle between peroxyl O–S bond vector and the SO_2 plane is 100°, with the OSOO angle equal to 100.1°). In MIN2, an incipient SO_3 moiety can be recognised and the charge density distribution on the two entities, SO_3 and HCO_3, is −0.83 e^- on the former and −0.17 e^- on the latter, therefore defining a sulphur trioxide anion and a bicarbonate radical. Proceeding along the reaction coordinate, MIN2 easily converts into MIN3, overcoming a barrier of only 5.7 kcal mol^{-1}. In TS23, the easy formation of an S–O bond and the breaking of the

O–O bond lead to a pyramidal SO_3 and an HCO_3 moiety. From this saddle point, a second oxygen atom is transferred from the carbonate to the sulphur trioxide moiety, forming an incipient sulphate in MIN3. This minimum is highly stabilised by 88.3 kcal mol^{-1} (Table 2) with respect to the entrance asymptote, thanks to the formation of a covalent S–O bond in the SO_3 moiety and to the strong interaction of the sulphur atom with the oxygen of the bicarbonate, preluding at the formation of a sulphate species. MIN3 is further stabilised by an intramolecular hydrogen bond, forming a six-membered ring. The charge density distribution of this stationary point is almost equally distributed between the SO_3 (-0.47 e^-) and HCO_3 (-0.53 e^-) groups; nonetheless, in MIN3, one can also consider a (distorted) tetrahedral SO_4 and a bent HCO_2 moiety. Therefore, two competing paths leading to the final products can be envisaged from this point. The first is the dissociation of MIN3 into HCO_3^- + SO_3 or into HCO_3 + SO_3^-, which is driven by the difference in AE between HCO_3 and SO_3. Accordingly, the exit path into HCO_3^- + SO_3 experimentally observed (reaction 2) largely prevails over the product couple HCO_3 + SO_3^-, accounting for the much higher electron affinity of the bicarbonate radical (EA $HCO_3^\bullet$ = 3.68 eV) [55] with respect to SO_3 (EA SO_3 = 1.90 eV [54], 2.22 eV [56]). The difference in the EA values of SO_3 is due to the uncertainty attached to the heat of formation of SO_3^- [54,56]. Accordingly, the enthalpy of reaction 3 is slightly positive (see also Table 2), which accounts for the low branching observed. A quite high dissociation energy of MIN3 (59.4 kcal mol^{-1}, Table 2) is required both to break the hydrogen bond and the S–O bond, and to change the SO_3 geometry from pyramidal to trigonal planar, to eventually release sulphur trioxide and the bicarbonate anion. This dissociation energy is, nevertheless, provided by the exothermicity of the process, calculated to be 28.9 kcal mol^{-1} (Table 2). Alternatively, MIN3 can isomerise with only 5.3 kcal mol^{-1} to the isoenergetic MIN4, a loose ion-neutral complex between the hydrogen sulphate anion and CO_2, from which only 8.1 kcal mol^{-1} is required to release the products. The products HSO_4^-/CO_2 are formed in a very exothermic process, calculated to be 80.9 kcal mol^{-1} (Table 2). Regarding the competition between the two product couples, HSO_4^-/CO_2 and HCO_3^-/SO_3, the experiments revealed a branching ratio of 3:1. Accordingly, the most stable HSO_4^-/CO_2 products are also formed through the faster path, occurring through a reaction coordinate developing well under the entrance asymptote, whereas HCO_3^-/SO_3, although forming from direct dissociation, requires a quite large amount of energy to attain the geometry of the products.

3. Discussion

Sulphur dioxide is effectively oxidised in the gas phase by the peroxymonocarbonate ion to hydrogen sulphate, sulphur trioxide, and, in a very minor amount, to SO_3^-. The reactions proceed through formal HOO^-, oxygen atom, and oxygen ion transfers, respectively. In the absence of solvent molecules, the reaction is found to proceed along a PES initially characterised by the formation of two encounter complexes (MIN1 and MIN2, Figure 4), in which the two reactants, SO_2 and HCO_4^-, maintain their geometric features and charge distribution. Nevertheless, the geometry of these adducts can be taken as a diagnostic of the bonding mode of sulphur dioxide, i.e., whether SO_2 behaves as a donor or acceptor molecule. In fact, in analogy with known complexes, metallic [46,47] or non-metallic [47], when SO_2 acts as a Lewis acid, it forms complexes with bent geometries, while linear geometries characterise SO_2, which behaves as a Lewis base.

In agreement, the coordination of HCO_4^- to SO_2 in MIN1 and MIN2 results in a bent geometry of the complexes (see Figure S3), the angle between the O-S bond vector and the plane of SO_2 moiety being around 100° in both structures, thereby qualifying SO_2 as a Lewis acid, accepting the lone pair of the oxygen atom in the OH group through its lowest unoccupied molecular orbital, and the interaction as $HCO_4^- \rightarrow SO_2$. The binding energies of the two minima, 12.7 and 15.7 kcal mol^{-1} (Figure 4, Table 2), are also in line with those calculated for complexes with pure donors, such as ammonia or methyl-substituted *N*-heterocyclic carbene, ranging from 10 kcal mol^{-1} ($NH_3 \cdot SO_2$) to 18 kcal mol^{-1} ($NHC \cdot SO_2$) [47]. Therefore, the Lewis acidic character of SO_2 discloses the

nucleophilic nature of HCO_4^-, which has rarely been observed in solution studies [20–22] when not questioned [14].

In solution, the generally accepted mechanism of the oxidation promoted by peroxymonocarbonate follows that of electrophilic peroxides [5]. The reaction occurs via a solvent-aided oxygen transfer mechanism, which involves a nucleophilic attack by the substrate, Nu, at the electrophilic oxygen of HCO_4^- with the formation of the oxidised substrate, NuO, and the bicarbonate ion. An example is given by the electrophilic oxidation of sulphides, substrates with clear nucleophilic properties, which selectively leads to sulfoxides [9]. Secondary oxidation to sulfones is due to $O_2^{\bullet -}$, generated upon the decomposition of HCO_4^-, or to H_2O_2, used to activate $NaHCO_3$, rather than the peroxymonocarbonate itself [14]. Much uncertainty regarding the nucleophilic behaviour of HCO_4^- still exists, also regarding the precise nature of the oxidant. Accordingly, the oxidative degradation of organophosphorus compounds, such as Paraoxon, in the $NaHCO_3$-activated H_2O_2 solutions appears to be attributable to HO_2^- or HO^- and not to HCO_4^- [14]. This problem is easily circumvented in the gas phase, where it is possible to select a precise oxidant, i.e., HCO_4^-, and study its reactivity towards a selected substrate, i.e., SO_2.

The actual oxidation step of the reaction occurs only in MIN3, in which one peroxidic oxygen atom has been fully transferred to sulphur dioxide, and the second one is still shared by the sulphur and carbon atoms. Accordingly, MIN3 can directly dissociate into HCO_3^- + SO_3 or into HCO_3 + SO_3^-, with a branching that reflects the thermodynamic stability of the products, or it can evolve, through a small barrier, to a loose ion-neutral complex, eventually leading to the separate products HSO_4^- + CO_2. Hence, the driving force of the major, highly exothermic, oxidation process is the liberation of the stable carbon dioxide molecule. This circumstance can explain the different reactivity observed in the reaction of the strong nucleophile hydroperoxide, HOO^-, which reacts with SO_2 at collision rate, forming SO_3^- and only a very small quantity of an adduct of formula $HOOSO_2^-$ and of unspecified structure [57].

Finally, the oxidation pathways described here show different characteristics compared to the SO_2 oxidation promoted by other anionic systems, such as oxyhalogenated ions (XO_n^- X = Cl, Br, I; n = 1,2) [42] or transition metal oxide anions (MO_2^-, M = Co, Ni, Cu, Zn; CrO_4^-) [37], whose common feature is that oxidation already occurs within the first highly exothermic intermediate, leading to free or bound $SO_3^{0/-}$. The same oxygen transfer process is not observed in the case of HCO_4^-, in which an intramolecular hydrogen bond engages the carbonyl oxygen in a stable 5-term cycle directing the reactivity towards the peroxidic OH that binds to SO_2. Oxidation is only observed when the peroxidic oxygen is no longer bound to the hydrogen atom and can be eventually transferred to SO_2.

4. Materials and Methods

4.1. Materials

The chemicals employed in this work were commercialised by Merck and used as received from the vendor. The stated purities are as follows: sodium percarbonate salt ($Na_2CO_3 \cdot 1.5\ H_2O_2$; avail. H_2O_2 20–30%), $Na_2{}^{13}CO_3$ (99 atom% ^{13}C), $NaH^{13}CO_3$ (98 atom% ^{13}C), $^{13}CO_2$ (99 atom% ^{13}C), and SO_2 (99.9%). All the solvents (H_2O HPLC grade, CH_3CN HPLC grade) were purchased from Carlo Erba Reagents S.r.l. and not further purified.

4.2. Mass Spectrometry

Mass spectrometric investigations were performed by using an LTQ-XL linear ion trap mass spectrometer (ThermoFisher Scientific, Waltham, MA, USA) equipped with an electrospray ionisation (ESI) source. This instrument was previously adapted to realise ion–molecule reaction (IMR) experiments [33,36–44]. Accordingly, the gaseous neutral reactant can be introduced into the ion trap through a deactivated fused silica capillary entering the vacuum chamber from a 6.25 mm hole placed in the backside of the mass spectrometer. A Granville-Phillips Series 370 Stabil Ion Vacuum Gauge was used to measure the pressure of the neutral gas, which was kept constant by a metering valve. Owing

to the position of the Pirani gauge compared to the ion trap, the actual gas pressure was obtained after reading calibrations [58]. The peroxymonocarbonate ion (HCO_4^-) was formed in solution by dissolving sodium percarbonate ($Na_2CO_3 \cdot 1.5\ H_2O_2$) in H_2O/CH_3CN (1:1, *v/v*) to a millimolar concentration, injected into the ESI source of the instrument at a flow rate of 5 μL min^{-1}. Alternatively, the HCO_4^- ion was obtained in the gas phase by directly subjecting pure water to the electrospray ionisation process. Nitrogen was used as a sheath and auxiliary gas at a flow rate of 11 and 2 arbitrary units (a. u.), respectively, a. u. ~0.37 L min^{-1}. Other source parameters were set as follows: spray voltage 3.2 kV, capillary temperature 275 °C, tube lens 15 V, and capillary voltage 10 V. Once optimised, the HCO_4^- reactant ion was isolated into the ion trap and exposed to gaseous sulphur dioxide (SO_2). Typical SO_2 pressures ranged between 1.1 × 10^{-7} Torr and 6.5 × 10^{-7} Torr, with uncertainty of ±30%. During the kinetic experiments, the normalised collision energy was set to zero, whereas the activation Q value was tuned to optimise the stable trapping fields for each ion. The ionic signals of the HCO_4^- reactant and reaction products were monitored over time as a function of the SO_2 concentration, and an average of 10 scans was acquired. Xcalibur 2.0.6 software was used to record and process all the mass spectra. Other selected neutrals, such as C_2H_4, $^{13}CO_2$, $C^{18}O_2$, CO, and O_2, proved unreactive with HCO_4^-. The reaction of HCO_4^- ion with gaseous SO_2 can be assimilated to a pseudo-first-order process due to the excess of neutral reactant compared to the precursor ion into the ion trap. Nonlinear least squares regression was performed by using the DynaFit4 software package [59], which simultaneously fit reactant and product concentrations vs. time. The reaction mechanism was verified by fitting the experimental results of the kinetic analysis with the mathematical model proposed for the postulated reaction, which simulated the time progress of the reaction based on the unimolecular rate constants obtained from the software calculations. The pseudo-first-order constants (s^{-1}) were divided into the concentrations of neutral reagent gas to derive the bimolecular rate constants k (cm^3 $molecule^{-1}$ s^{-1}), whereas the branching ratios of the different reaction channels were obtained from the formation constants of the direct products. According to the average dipole orientation (ADO) theory [60], the efficiency of the process was calculated as the ratio of the bimolecular rate constant k to the collision rate constant (k_{coll}). Approximately 15 independent measurements were performed on different days over a sixfold neutral pressure range to guarantee the linearity of the k values. The standard deviation in the absolute rate constant was typically <10%, although a conservative error of 30% was given owing to the uncertainties affecting the measurement of the neutral pressure. The ionic reactant and products were also characterised by collision-induced dissociation (CID) experiments performed by furnishing energy to mass-selected ions in the presence of helium background gas (P He ca. 3 × 10^{-3} Torr). Normalised collision energies were tuned in a 20–40% range as a function of the isolated species and applied with a standard activation time of 30 ms. Ions were mass-selected with a window of 1 *m/z* and a Q value optimised to ensure stable trapping fields for all the ionic species under investigation.

The ^{13}C-labelled experiments were performed by preparing and mass-analysing millimolar solutions of $Na_2{}^{13}CO_3$ or $NaH^{13}CO_3$ salt. Analogous studies were also carried out on 1.5 mL of ultrasound-degassed water placed in a double bottle-neck flask that was filled with $^{13}CO_2$ until a pressure of 700 torr.

4.3. Computational Details

The potential energy surface of the system [$HCO_4^- \cdots SO_2$] was investigated localising the lowest stationary points at the B3LYP [61,62] level of theory in conjunction with the correlation consistent valence polarised set aug-cc-pVTZ [63–65], augmented with a tight *d* function with exponent 2.457 for the sulphur atom [66], to correct for the core polarisation effects [67]. This basis set will be denoted aug-cc-pV(T+d)Z. At the same level of theory, we computed the harmonic vibrational frequencies in order to check the nature of the stationary points, i.e., minimum if all the frequencies are real, saddle point if there is one, and only one for the imaginary frequency. The energy of all the stationary points was

computed at the higher level of calculation CCSD(T) [68–70] using the same basis set, aug-cc-pV(T+d)Z. Both the B3LYP and the CCSD(T) energies were corrected to 298.15 K by adding the zero point energy and the thermal corrections computed using the scaled harmonic vibrational frequencies evaluated at the B3LYP/aug-cc-pV(T+d)Z level. All calculations were performed using Gaussian 09 [71], while the analysis of the vibrational frequencies was performed using Molekel [72,73].

5. Conclusions

Sulphur dioxide is efficiently oxidised in the gas phase by the peroxymonocarbonate ion, HCO_4^-, through the formal transfer of HO_2^-, oxygen atom, and oxygen ion, to the hydrogen sulphate anion, sulphur trioxide, and sulphur trioxide anion, respectively. Secondary reactions due to the formation of the hydrogen carbonate anion lead to the formation of hydrogen sulphite. The three oxidative pathways have been characterised using a joint approach of mass spectrometry and theoretical calculations. Contrary to the common behaviour observed in solution, in the gas phase, the peroxymonocarbonate exhibits nucleophilic properties, which are unravelled by the Lewis acid character of sulphur dioxide.

Supplementary Materials: The following supporting information can be downloaded at: https://www.mdpi.com/article/10.3390/molecules28010132/s1, Figure S1: Ion–molecule reaction of isolated $H^{13}CO_4^-$ ions with SO_2. Figure S2: Complete geometrical parameters of minima and saddle points relative to the HCO_4^- + SO_2 PES; Figure S3: Details of MIN1 and MIN2.

Author Contributions: Conceptualisation, G.d.P., A.T., M.R.; methodology, A.T., M.R., C.S.; investigation, C.S.; data curation, A.T., M.R., C.S.; validation, A.T., F.P., C.S.; writing—original draft preparation, A.T., G.d.P., C.S., M.R.; writing—review and editing, A.T., G.d.P., M.R., C.S., F.P.; funding acquisition, G.d.P., A.T., M.R. All authors have read and agreed to the published version of the manuscript.

Funding: This research was supported by Università degli Studi di Rome Sapienza "Progetti di Ateneo" (Project No. RM12117A5CEA4803) and by Università degli Studi di Perugia ("Fondo Ricerca di Base 2019"). C.S. thanks the Italian Ministry of University and Research (MUR) for a Researcher position (DM 1062, 10/08/2021) within the EU-funded National Operational Program (PON) on Research and Innovation 2014–2020.

Institutional Review Board Statement: Not applicable.

Informed Consent Statement: Not applicable.

Data Availability Statement: Not applicable.

Acknowledgments: The authors thank the Dipartimento di Ingegneria Civile ed Ambientale-Università degli Studi di Perugia for the allocated computing time within the project "Dipartimenti di Eccellenza 2018–2022".

Conflicts of Interest: The authors declare no conflict of interest.

Sample Availability: Not applicable.

References

1. Giguère, P.A.; Lemaire, D. Etude spectroscopique des dérivés du peroxyde d'hydrogène. V. Les percabonates $KHCO_4$ et $K_2C_2O_6$. *Can. J. Chem.* **1972**, *50*, 1472–1476. [CrossRef]
2. Jones, P.; Griffith, W.P. Alkali-metal Peroxocarbonates, $M_2[CO_3]_nH_2O_2$, $M_2[C_2O_6]$, $M[HCO_4]\cdot_nH_2O$ and $Li_2[CO_4]\cdot H_2O$. *J. Chem. Soc. Dalton Trans.* **1980**, *12*, 2526–2532. [CrossRef]
3. Flanagan, J.; Jones, D.P.; Griffith, W.P.; Skapski, A.C.; West, A.P. On the existence of peroxocarbonates in aqueous solution. *J. Chem. Soc. Chem. Commun.* **1986**, *1*, 20–21. [CrossRef]
4. Adam, A.; Mehta, M. $KH(O_2)CO_2\cdot H_2O_2$-An oxygen-rich salt of monoperoxocarbonic acid. *Angew. Chem. Int. Ed.* **1998**, *37*, 1387–1388. [CrossRef]
5. Swern, D. *Organic Peroxides*; Wiley: New York, NY, USA, 1970; pp. 313–516.
6. Bakhmutova-Albert, E.V.; Yao, H.; Denevan, D.E.; Richardson, D.E. Kinetics and mechanism of peroxymonocarbonate formation. *Inorg. Chem.* **2010**, *49*, 11287–11296. [CrossRef]

7. Yao, H.; Richardson, D.E. Epoxidation of alkenes with bicarbonate-activated hydrogen peroxide. *J. Am. Chem. Soc.* **2000**, *122*, 3220–3221. [CrossRef]
8. Balagam, B.; Richardson, D.E. The mechanism of carbon dioxide catalysis in the hydrogen peroxide N-Oxidation of amines. *Inorg. Chem.* **2008**, *47*, 1173–1178. [CrossRef] [PubMed]
9. Richardson, D.E.; Yao, H.; Frank, K.M.; Bennett, D.A. Equilibria, kinetics, and mechanism in the bicarbonate activation of hydrogen peroxide: Oxidation of sulphides by peroxymonocarbonate. *J. Am. Chem. Soc.* **2000**, *122*, 1729–1739. [CrossRef]
10. Bennet, D.A.; Yao, H.; Richardson, D.E. Mechanism of sulphide oxidations by peroxymonocarbonate. *Inorg. Chem.* **2001**, *40*, 2996–3001. [CrossRef]
11. Richardson, D.E.; Regino, C.A.S.; Yao, H.; Johnson, J.V. Methionine oxidation by peroxymonocarbonate, a reactive oxygen species formed from CO_2/bicarbonate and hydrogen peroxide. *Free Radic. Biol. Med.* **2003**, *35*, 1538–1550. [CrossRef]
12. Regino, C.A.S.; Richardson, D.E. Bicarbonate-catalyzed hydrogen peroxide oxidation of cysteine and related thiols. *Inorg. Chim. Acta* **2007**, *360*, 3971–3977. [CrossRef]
13. Yang, X.; Duan, Y.; Wang, J.; Wang, H.; Liu, H.; Sedlak, D.L. Impact of peroxymonocarbonate on the transformation of organic contaminants during hydrogen peroxide in situ chemical oxidation. *Environ. Sci. Technol. Lett.* **2019**, *6*, 781–786. [CrossRef] [PubMed]
14. Zhao, S.; Xi, H.; Zuo, Y.; Wang, Q.; Wang, Z.; Yan, Z. Bicarbonate-activated hydrogen peroxide and efficient decontamination of toxic sulfur mustard and nerve gas simulants. *J. Hazard Mater.* **2018**, *344*, 136–145. [CrossRef] [PubMed]
15. Pan, H.; Gao, Y.; Li, N.; Zhou, Y.; Lin, Q.; Jiang, J. Recent advances in bicarbonate-activated hydrogen peroxide system for water treatment. *Chem. Eng. J.* **2021**, *408*, 127332. [CrossRef]
16. Medinas, D.B.; Cerchiaro, G.; Trindade, D.F.; Augusto, O. The Carbonate Radical and Related Oxidants Derived from Bicarbonate Buffer. *IUBMB Life* **2007**, *59*, 255–262. [CrossRef]
17. Radi, R. Interplay of carbon dioxide and peroxide metabolism in mammalian cells. *J. Biol. Chem.* **2022**, *298*, 102358. [CrossRef]
18. Francioso, A.; Baseggio Conrado, A.; Blarzino, C.; Foppoli, C.; Montanari, E.; Dinarelli, S.; Giorgi, A.; Mosca, L.; Fontana, M. One- and two-electron oxidations of β-Amyloid$_{25\text{-}35}$ by carbonate radical anion ($CO_3^{\cdot -}$) and peroxymonocarbonate (HCO_4^-): Role of sulfur radical reactions in peptide aggregation. *Molecules* **2020**, *25*, 961. [CrossRef]
19. Zhang, H.; Joseph, J.; Gurney, M.; Becker, D.; Kalyanaraman, B. Bicarbonate Enhances Peroxidase Activity of Cu, Zn-Superoxide Dismutase. *J. Biol. Chem.* **2002**, *277*, 1013–1020. [CrossRef]
20. Savelova, V.A.; Popov, A.F.; Vakhitova, L.N.; Solomoichenko, T.N.; Sadovskii, Y.S.; Prokop'eva, T.M.; Skrypka, A.V.; Panchenko, B.V. Nucleophilic reactivity of hydroxide and hydroperoxide ions in aqueous-alcoholic media and of HCO_4^- ion in water. *Russ. J. Org. Chem.* **2005**, *41*, 1773–1781. [CrossRef]
21. Savelova, V.A.; Sadovskii, Y.S.; Solomoichenko, T.N.; Prokop'eva, T.M.; Kosmynin, V.V.; Piskunova, Z.P.; Bunton, C.A.; Popov, A.F. Nucleophilic activity of peroxyhydrocarbonate and peroxocarbonate ions relative to 4-nitrophenyl diethyl phosphonate. *Theor. Exp. Chem.* **2008**, *44*, 101–108. [CrossRef]
22. Vakhitova, L.N.; Matvienko, K.V.; Taran, N.A.; Lakhtarenko, N.V.; Popov, A.F. Nucleophilic Oxidizing Systems Based on Hydrogen Peroxide for Decomposition of Ecotoxicants. *Russ. J. Org. Chem.* **2011**, *47*, 965–973. [CrossRef]
23. Attiogbe, F.K.; Bose, S.K.; Wang, W.; McNeillie, A.; Francis, R.C. The peroxymonocarbonate anions as pulp bleaching agents. Part 1. Results with lignin model compounds and chemical pulps. *BioResources* **2010**, *5*, 2208–2220. [CrossRef]
24. Wincel, H.; Mereand, E.; Castleman, A.W. Gas-Phase Reactions of $HO_2^{\cdot -}CO_2$ with Molecular Species of Possible Atmospheric Interest. *J. Phys. Chem.* **1995**, *99*, 6601–6607. [CrossRef]
25. Bohme, D.K.; Goodings, J.M.; Ng, C.-W. In situ chemical ionization as a probe for neutral constituents upstream in a methane-oxygen flame. *Int. J. Mass Spectrom. Ion Phys.* **1977**, *24*, 335–354. [CrossRef]
26. McAllister, T.; Nicholson, A.J.C.; Swingler, D.L. Negative ions in the flame ionization detector and the occurrence of HCO_4^-. *Int. J. Mass Spectrom. Ion Phys.* **1978**, *27*, 43–48. [CrossRef]
27. Cody, R.B.; Laramee, J.A.; Durst, H.D. Versatile new ion source for the analysis of materials in open air under ambient conditions. *Anal. Chem.* **2005**, *77*, 2297–2302. [CrossRef]
28. Ninomiya, S.; Iwamoto, S.; Usmanov, D.T.; Hiraoka, K.; Yamabe, S. Negative-mode mass spectrometric study on dc corona, ac corona and dielectric barrier discharge ionization in ambient air containing H_2O_2, 2,4,6-trinitrotoluene (TNT), and 1,3,5-trinitroperhydro-1,3,5-triazine (RDX). *Int. J. Mass Spectrom.* **2021**, *459*, 116440. [CrossRef]
29. Sekimoto, K.; Takayama, M. Observation of different core water cluster ions $Y^-(H_2O)_n$ (Y = O_2, HO_x, NO_x, CO_x) and magic number in atmospheric pressure negative corona discharge mass spectrometry. *J. Mass Spectrom.* **2011**, *46*, 50–60. [CrossRef]
30. O'Hair, R.A.J. The 3D quadrupole ion trap mass spectrometer as a complete chemical laboratory for fundamental gas-phase studies of metal mediated chemistry. *Chem. Comm.* **2006**, *14*, 1469–1481. [CrossRef]
31. Osburn, S.; Ryzhov, V. Ion−Molecule Reactions: Analytical and Structural Tool. *Anal. Chem.* **2013**, *85*, 769–778. [CrossRef]
32. Schwarz, H. Ménage-à-trois: Single-atom catalysis, mass spectrometry, and computational chemistry. *Catal. Sci. Technol.* **2017**, *7*, 4302–4314. [CrossRef]
33. Troiani, A.; Rosi, M.; Garzoli, S.; Salvitti, C.; de Petris, G. Iron-Promoted C-C Bond Formation in the Gas Phase. *Angew. Chem. Int. Ed.* **2015**, *54*, 14359–14362. [CrossRef] [PubMed]
34. Mueller, H. *Ullmann's Encyclopedia of Industrial Chemistry*; Wiley-VCH: Weinheim, Germany, 2000.

35. Smith, S.J.; Pitcher, H.; Wigley, T.M. Global and regional anthropogenic sulfur dioxide emissions. *Glob. Planet. Chang.* **2001**, *29*, 99–119. [CrossRef]
36. Troiani, A.; Rosi, M.; Garzoli, S.; Salvitti, C.; de Petris, G. Effective redox reactions by chromium oxide anions: Sulfur dioxide oxidation in the gas phase. *Int. J. Mass Spectrom.* **2019**, *436*, 18–22. [CrossRef]
37. Salvitti, C.; Rosi, M.; Pepi, F.; Troiani, A.; de Petris, G. Reactivity of transition metal dioxide anions MO_2^- (M = Co, Ni, Cu, Zn) with sulfur dioxide in the gas phase: An experimental and theoretical study. *Chem. Phys. Lett.* **2021**, *776*, 138555. [CrossRef]
38. Salvitti, C.; Pepi, F.; Troiani, A.; de Petris, G. Regioselective Bond-Forming and Hydrolysis Reactions of Doubly Charged Vanadium Oxide Anions in the Gas Phase. *Reactions* **2022**, *3*, 254–264. [CrossRef]
39. Troiani, A.; Rosi, M.; Garzoli, S.; Salvitti, C.; de Petris, G. Vanadium hydroxyde cluster ions in the gas-phase: Bond-forming reactions of doubly-charged negative ions by SO_2-promoted V-O activation. *Chem. Eur. J.* **2017**, *23*, 11752–11756. [CrossRef]
40. Troiani, A.; Rosi, M.; Garzoli, S.; Salvitti, C.; de Petris, G. Sulphur dioxide cooperation in hydrolysis of vanadium oxide and hydroxide cluster dianions. *N. J. Chem.* **2018**, *42*, 4008–4016. [CrossRef]
41. De Petris, G.; Cartoni, A.; Troiani, A.; Angelini, G.; Ursini, O. Water activation by SO_2^+ ions: An effective source of OH radicals. *Phys. Chem. Chem. Phys.* **2009**, *11*, 9976–9978. [CrossRef]
42. Troiani, A.; Rosi, M.; Salvitti, C.; de Petris, G. The oxidation of sulfur dioxide by single and double oxygen transfer paths. *Chem. Phys. Chem.* **2014**, *15*, 2723–2731. [CrossRef]
43. Troiani, A.; Salvitti, C.; de Petris, G. Gas-phase reactivity of carbonate ions with sulfur dioxide: An experimental study of cluster reactions. *J. Am. Chem. Soc. Mass Spectrom.* **2019**, *30*, 1964–1972. [CrossRef] [PubMed]
44. Salvitti, C.; Pepi, F.; Troiani, A.; de Petris, G. Intracluster sulphur dioxide oxidation by sodium chlorite anions: A mass spectrometric study. *Molecules* **2021**, *26*, 7114. [CrossRef] [PubMed]
45. Li, J.; Rogachev, A.Y. SO_2—Yet another two-faced ligand. *Phys. Chem. Chem. Phys.* **2015**, *17*, 1987–2000. [CrossRef] [PubMed]
46. Oh, J.J.; La Barge, M.S.; Matos, J.; Kampf, J.W.; Hilling II, K.W.; Kuczkowski, R.L. Structure of the Trimethylamine-Sulfur Dioxide Complex. *J. Am. Chem. Soc.* **1991**, *113*, 4732–4738. [CrossRef]
47. Kubas, G.J. Diagnostic Features of Transition-Metal-SO_2 Coordination Geometries. *Inorg. Chem.* **1979**, *18*, 182–188. [CrossRef]
48. Fehsenlfeld, F.C.; Ferguson, E.E. Laboratory studies of negative ion reactions with atmospheric trace constituents. *J. Chem. Phys.* **1974**, *61*, 3181–3193. [CrossRef]
49. Van Berkel, G.J.; Kertesz, V. Using the Electrochemistry of the Electrospray Ion Source. *Anal. Chem.* **2007**, *79*, 5510–5520. [CrossRef] [PubMed]
50. Hvelplund, P.; Kadhane, U.; Nielsen, S.B.; Panja, S.; Støchkel, K. On the formation of water-containing negatively charged clusters from atmospheric pressure corona discharge in air. *Int. J. Mass Spectrom.* **2010**, *292*, 48–52. [CrossRef]
51. Tinke, A.P.; Heeremans, C.E.M.; van der Hoeven, R.A.M.; Niessen, W.M.A.; van der Greef, J.; Nibbering, N.M.M. Positively and negatively charged water cluster ions generated via liquid chromatography/thermospray mass spectrometry. *Rapid Comm. Mass Spectrom.* **1991**, *5*, 188–191. [CrossRef]
52. Yang, X.; Castleman Jr, A.W. Reactions of O_2H^- and its hydrates with CH_3CN, CO_2 and SO_2. *Chem. Phys. Lett.* **1991**, *179*, 361–366. [CrossRef]
53. England, A.H.; Duffin, A.M.; Schwartz, C.P.; Uejio, J.S.; Prendergast, D.; Saykally, R.J. On the hydration and hydrolysis of carbon dioxide. *Chem. Phys. Lett.* **2011**, *514*, 187–195. [CrossRef]
54. *Chemistry WebBook*; NIST Standard Reference Database Number 69; Linstrom, P.; Mallar, W., Eds. National Institute of Standards and Technology: Gaithersburg, MD, USA, 2022. [CrossRef]
55. Wang, X.-B.; Xantheas, S.S. Photodetachment of isolated bicarbonate anion: Electron binding energy of HCO_3^-. *J. Phys. Chem. Lett.* **2011**, *2*, 1204–1210. [CrossRef] [PubMed]
56. Ruscic, B.; Bross, D.H. *Active Thermochemical Tables (ATcT) Values Based on ver. 1.122q of the Thermochemical Network*; Argonne National Laboratory: Lemont, IL, USA, 2021. Available online: https://atct.anl.gov/ (accessed on 15 December 2022). [CrossRef]
57. Bowie, J.H.; DePuy, C.H.; Sullivan, S.A.; Bierbaum, V.M. Gas phase reactions of the hydroperoxide and peroxyformate anions. *Can. J. Chem.* **1986**, *64*, 1046–1050. [CrossRef]
58. Bartmess, J.E.; Georgiadis, R. Empirical methods for determination of ionization gauge relative sensitivities for different gases. *Vacuum* **1983**, *33*, 149–153. [CrossRef]
59. Kuzmic, P. Program DYNAFIT for the Analysis of Enzyme Kinetic Data: Application to HIV Proteinase. *Anal. Biochem.* **1996**, *237*, 260–273. [CrossRef] [PubMed]
60. Bowers, M.T.; Su, T. *Interactions between Ions and Molecules*; Plenum Press: New York, NY, USA, 1975.
61. Becke, A.D. A new mixing of Hartree–Fock and local density-functional theories. *J. Chem. Phys.* **1993**, *98*, 1372–1377. [CrossRef]
62. Stephens, P.J.; Devlin, F.J.; Chablowski, C.F.; Frisch, M.J. Ab Initio Calculation of Vibrational Absorption and Circular Dichroism Spectra Using Density Functional Force Fields. *J. Phys. Chem.* **1994**, *98*, 11623–11627. [CrossRef]
63. Dunning, T.H., Jr. Gaussian basis sets for use in correlated molecular calculations. I. The atoms boron through neon and hydrogen. *J. Chem. Phys.* **1989**, *90*, 1007–1023. [CrossRef]
64. Woon, D.E.; Dunning, T.H., Jr. Gaussian basis sets for use in correlated molecular calculations. III. The atoms aluminum through argon. *J. Chem. Phys.* **1993**, *98*, 1358–1371. [CrossRef]
65. Kendall, R.A.; Dunning, T.H., Jr.; Harrison, J.R. Electron affinities of the first-row atoms revisited. Systematic basis sets and wave functions. *J. Chem. Phys.* **1992**, *96*, 6796–6806. [CrossRef]

66. Bauschlicher, C.W., Jr.; Partridge, H. The sensitivity of B3LYP atomization energies to the basis set and a comparison of basis set requirements for CCSD(T) and B3LYP. *Chem. Phys. Lett.* **1995**, *240*, 533–540. [CrossRef]
67. Martin, J.M.L.; Uzan, O. Basis set convergence in second-row compounds. The importance of core polarization functions. *Chem. Phys. Lett.* **1998**, *282*, 16–24. [CrossRef]
68. Bartlett, R.J. Many-Body Perturbation Theory and Coupled Cluster Theory for Electron Correlation in Molecules. *Annu. Rev. Phys. Chem.* **1981**, *32*, 359–401. [CrossRef]
69. Raghavachari, K.; Trucks, G.W.; Pople, J.A.; Head-Gordon, M. A fifth-order perturbation comparison of electron correlation theories. *Chem. Phys. Lett.* **1989**, *157*, 479–483. [CrossRef]
70. Olsen, J.; Jorgensen, P.; Koch, H.; Balkova, A.; Bartlett, R.J. Full configuration–interaction and state of the art correlation calculations on water in a valence double-zeta basis with polarization functions. *J. Chem. Phys.* **1996**, *104*, 8007–8015. [CrossRef]
71. Frisch, M.J.; Trucks, G.W.; Schlegel, H.B.; Scuseria, G.E.; Robb, M.A.; Cheeseman, J.R.; Scalmani, G.; Barone, V.; Mennucci, B.; Petersson, G.A.; et al. *Gaussian 09, Revision A.02*; Gaussian, Inc.: Wallingford, CT, USA, 2009.
72. Flükiger, P.; Lüthi, H.P.; Portmann, S.; Weber, J. MOLEKEL. version 4.3. Swiss Center for Scientific Computing: Manno, Switzerland, 2000.
73. Portmann, S.; Lüthi, H.P. MOLEKEL: An Interactive Molecular Graphics Tool. *Chimia* **2000**, *54*, 766–769. [CrossRef]